*Int. J. Electrochem. Sci.*, 14 **(2019)** 8699 – 8708, doi: 10.20964/2019.09.09

International Journal of
ELECTROCHEMICAL
SCIENCE
www.electrochemsci.org

*Short Communication*

# Corrosion and Electrochemical Impedance Properties of Ti6Al4V Alloy and Ti-3Zr-2Sn-3Mo-25Nb Alloy Treated by Micro-arc Oxidation Process

*Mei Yang*[1,*], *Wenhao Zhang*[1], *Jin Chen*[2], *Yang Li*[2], *Tingyu Huang*[1], *Ning Tang*[1], *Pengcheng Li*[1]

[1] Materials Science and Engineering, Southwest Petroleum University, Cheng'du 610500, China
[2] Sichuan petroleum Enginering Construction Co.,Ltd, Cheng'du 610000, China
[*]E-mail: 380056676@qq.com

*Received:* 19 April 2019 / *Accepted:* 18 June 2019 / *Published:* 31 July 2019

To analyse the effects of micro-arc oxidation (MAO) on the different substrates, TLM (Ti-3Zr-2Sn-3Mo-25Nb) and TC4 (Ti-6Al-4V) were oxidized in an aqueous electrolyte including $KH_2PO_4$, $Ca(CH_3COO)_2$ and EDTA-2Na. The bore diameters of the two kinds of material were both between 0.5 and 2 μm in ceramic film surfaces. The MAO coatings consisted of two layers: a dense inner layer and a porous outer layer. The TLM-MAO coating included anatase, rutile, CaP and $Nb_2O_5$, whereas the TC4-MAO coating included anatase, rutile, CaP and brookite. The Ca and P contents of the TLM-MAO coating were higher than those of TC4, which had better biocompatibility. Furthermore, the corrosion resistance of the two kinds of coatings was estimated by potentiodynamic polarization curves and the electrochemical impedance spectrum in SBF(simulated body fluid). By analysing the self-corrosion current density, impedance and equivalent circuit model, it was found that the corrosion resistance of the TC4 micro-arc oxidation coating, which mainly depends on the dense layer, is better than that of the TLM-MAO sample.

**Keywords:** Micro arc oxidation; Corrosion resistance; Coating

## 1. INTRODUCTION

Pure titanium and its alloys have received more attention in the aviation filed and the semiconductor and clinical medicine industries[1-2], because of their distinguished combination of properties, such as high corrosion resistance and excellent biocompatibility of their surfaces[3-4]. Nevertheless, titanium and its alloys that are applied in clinical medicine still do not meet expectations because of the obvious contact corrosion of these materials[5]. Titanium alloys have thin and porous natural oxide films[6], and once these materials are exposed to body fluids, a small amount of metal ions lead to cell toxicity and inflammation, resulting in failure of the implant[7]. To enhance the

corrosion resistance of titanium and titanium alloys in the field of clinical medicine, it is necessary to modify the composition and performance of the titanium alloy surfaces.

To date, many surface technologies have been applied on the surface of titanium alloys to improve corrosion resistance, including physical and chemical deposition (PVD and CVD), plasma spraying, anodic oxidation and micro-arc oxidation (MAO)[8-9]. Among them, micro-arc oxidation also referred to as micro-plasma oxidation, has considerable application prospects due to its high efficiency, high performance cost ratio and environmentally-friendly cutting-edge technology for valve metals and their alloys[10]. In the process, the phase composition, structure and physical or chemical properties of the surface will be changed[11-12].

Ti-3Zr-2Sn-3Mo-25Nb (TLM) titanium alloys, as a medical near-β-type titanium alloy, show good elastic deformation behaviour, similar to human bone[13]. In this paper, the widely used Ti-6Al-4V (TC4) alloy and Ti-25Nb-3Zr-2Sn-3Mo (TLM) alloy are compared to analyse the morphology, structure and corrosion resistance of micro-arc oxidation films.

## 2. EXPERIMENT

### *2.1Materials and preparation of oxide coating*

A biomimetic alloy (Ti-3Zr-2Sn-3Mo-25Nb) with dimensions of ∅13 mm ×2 mm and the TC4 titanium alloy (10 mm×10 mm×15 mm) were used as substrates. Before oxidation, the surfaces of the samples were ground with fine SiC sandpaper, degreased ultrasonically and washed with ethanol and deionized water. In our previous study, we determined a series of micro-arc oxidation parameters to improve the biocompatibility of the oxidized coatings. Micro-arc oxidation with the prepared substrates and the corrosion-resistant plate as the anode and cathode, respectively, was performed under constant current conditions in an aqueous electrolyte containing $KH_2PO_4$, $Ca(CH_3COO)_2$ and EDTA-2Na. The electrolyte temperature was maintained at room temperature by a heat exchange system. During the oxidation process, the frequency was 100 Hz, with a duty ratio of 30%, and the oxidation time was maintained for 30 minutes. After oxidation, the substrates were immersed in hot water at 90°C for a few minutes and dried in a dry air stream.

### *2.2 Characterization of the coating*

The phase composition of the treated surface was determined by X-ray diffraction (XRD, DX-2700B), which was carried out over a scanning range ($2\theta$) from 10° to 80° at a scanning rate of 0.04°/s. The coatings and cross-sectional morphologies of the samples were observed by scanning electron microscopy (SEM, FEI Quanta 450). Electrochemical experiments included electrochemical impedance spectroscopy (EIS) and potentiodynamic polarization tests, which were performed using AUTOLAB PGSTAT 302N from Metrohm Instruments. A three-electrode system was adopted during the process of corrosion, consisting of a platinum electrode, a saturated calomel electrode (reference electrode) and a sample (working electrode). The potential scan rate in the potentiodynamic tests was 1

mV/s, starting at -1 V below the OCP and moving in the anodic direction up to 1 V. The frequency range in the electrochemical impedance test is $10^{-2}$ ~ $10^{5}$ Hz. Then, the electrochemical impedance data and polarization curve were analysed by ZSimDemo and CorrView software, respectively. In the SBF (table 1), the corrosion test was carried out at a pH of 7.4 and a temperature of 37°C.

**Table 1.** The chemical composition of SBF solution (g/L)

| Name | NaCl | KCl | $NaHCO_3$ | $CaCl_2$ | $Na_2HPO_4$ | $KH_2PO_4$ | $MgSO_4{\cdot}7H_2O$ | Glucose |
|---|---|---|---|---|---|---|---|---|
| Compose (g/L) | 8 | 0.4 | 0.35 | 0.14 | 0.06 | 0.06 | 0.2 | 1 |

## 3. RESULTS AND DISCUSSION

### *3.1 Phase and morphology*

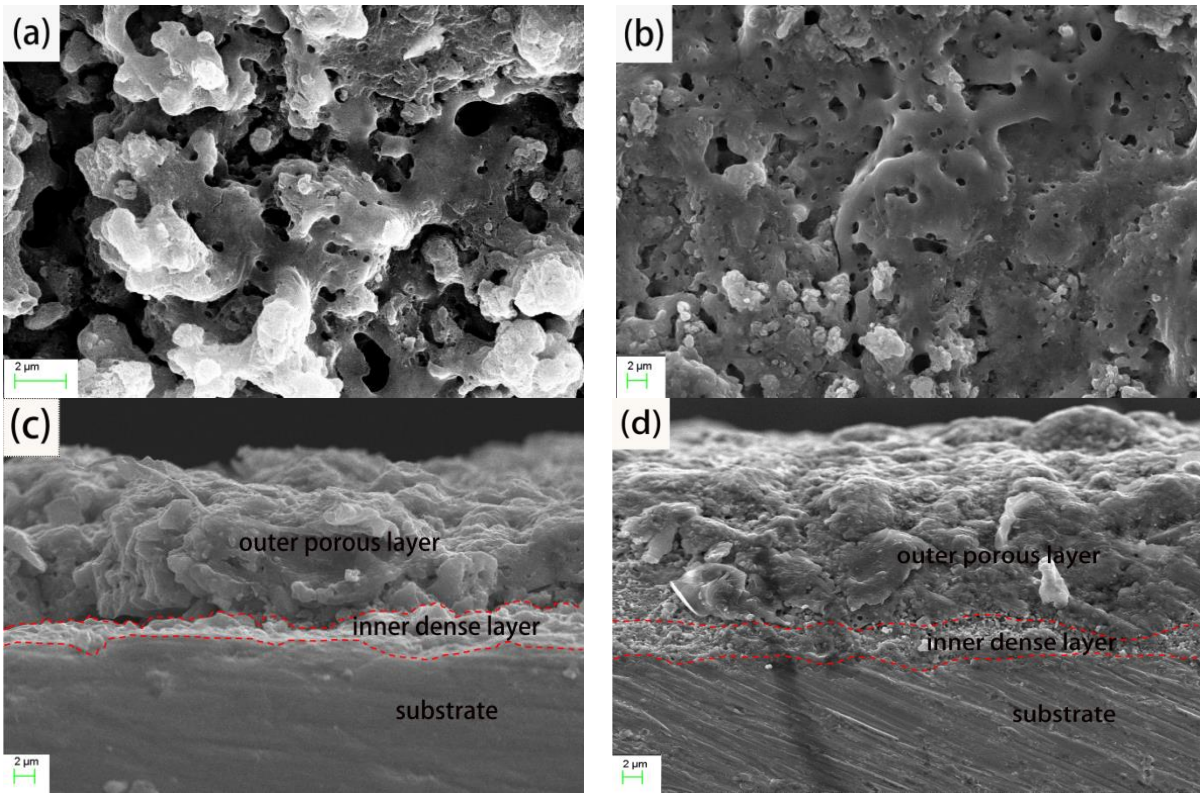


**Figure 1.** SEM images of different alloys: (a) TC4-MAO, (b) TLM-MAO coatings and cross-sectional coatings: (c) TC4-MAO, (d) TLM-MAO at 25°C.

The surface morphologies of the MAO coatings of TC4 and TLM are presented in Fig. 1(a), (b), respectively. As observed, there is no significant difference between the two kinds of micro-arc oxide films on the surface of titanium alloys. The porous structure and some granular melting sinters are presented on the surface of the treated samples, and the diameter of the holes is between

approximately 0.5 and 2 μm. The size of these pores depends on the pulse energy, the amount of discharge sparks and the growth rate of the oxide layer during the micro arc oxidation process. MAO coatings are highly dependent on the electrical parameters and electrolyte composition[14]. In the experiment, the preparation process and parameters of the two micro-arc oxidation layers are similar, so there is little difference.

Figs. 1(c) and (d) show the cross-sectional coatings of the two alloys. By comparing the brightness of different parts, the films can be clearly divided into two layers: a dense inner layer and a porous outer layer. The thickness of the inner layer is approximately 7 μm, and the outer layer is approximately 62.5 μm. However, the micro-arc oxidation layer of TLM is more uniform than that of TC4, which is beneficial for improving the properties of the alloy.

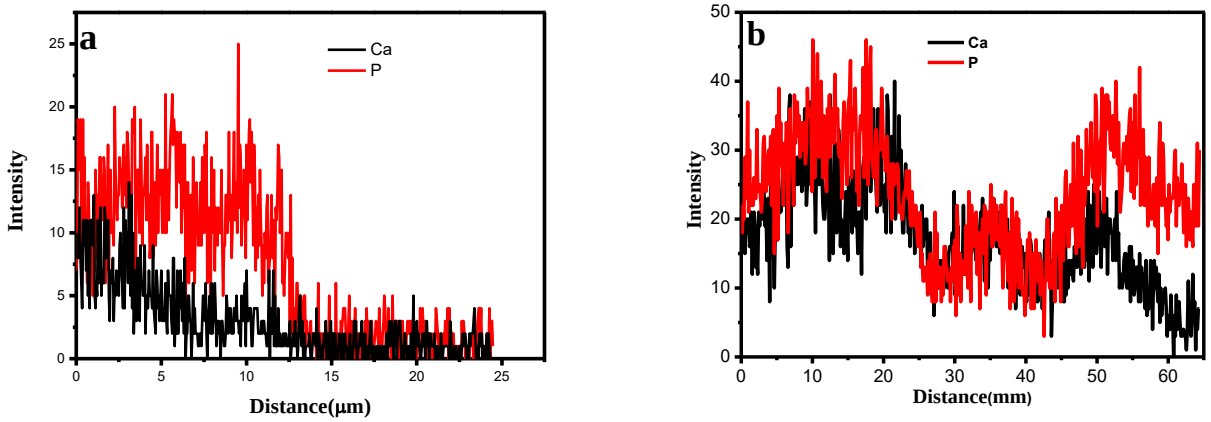


**Figure 2.** P and Ca element line distributions of the cross-sectional coating: (a) TC4, (b) TLM at 25°C.

Fig. 2 shows the elemental line distribution of the cross-section of the coatings. Maximum contents of calcium and phosphorus occur on the surface, which are the main elements in the formation of hydroxyapatite. Farther from the coating surface, the content of phosphorus is greater than that of the calcium. It can be assumed that ions in the electrolyte enter the discharge channel by electrophoresis and diffusion. The $Ca^{2+}$ in the electrolyte leaves the anode due to the effect of the electric field, while $PO_4^{3-}$ exists more on the anode. Therefore, the concentration of $PO_4^{3-}$ in the coating surface will be greater than that of $Ca^{2+}$ when the coating is initially formed. With increasing oxidation time, the concentration of $PO_4^{3-}$ tends to be stable, and the $Ca^{2+}$ moves to the anode due to the concentration gradient. Therefore, the calcium content increases during the micro-arc oxidation process. According to table 2, the content of Ca in the TC4 alloy is lower than that in the TLM alloy, probably due to the presence of $Al^{3+}$ in TC4, which prevents the formation of $CaY^{2-}$ by producing $AlY^{3-}$ ($Y=[2(OOCCH_2)NCH_2CH_2N(CH_2COO)_2]^{4-}$)[15], decreasing the ion mobility of $Ca^{2+}$ during electrophoresis.

**Table 2.** The relative content of elements on the coating cross section by EDS (wt%)

| Name | O | P | K | Ca | Ti | Nb | Al | V |
|---|---|---|---|---|---|---|---|---|
| TC4 | 23.13 | 13.90 | - | 18.24 | 39.58 | - | 3.87 | 1.28 |
| TLM | 17.89 | 14.31 | 0.34 | 28.55 | 29.19 | 9.72 | - | - |

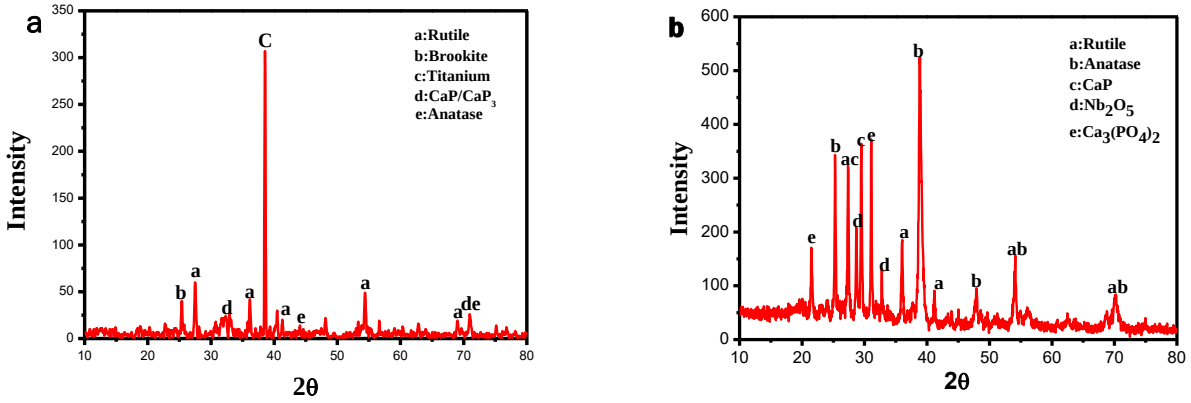


**Figure 3.** XRD spectra of MAO coatings prepared with different substrates: (a) TC4 and (b) TLM at room temperature.

The XRD pattern of the micro-arc oxidation coatings is shown in Fig. 3. The TC4-MAO coating exhibits a weaker peak than the TLM-MAO coating. Thus, the preferred orientation of the cell can be assumed. In Fig. 3(a), rutile, anatase, brookite and CaP appear on the TC4-MAO coating. Aluminium and vanadium oxides are undetected due to their low contents. In Fig. 3(b), XRD diffraction analysis indicates that the coating consists mainly of anatase, rutile and CaP. In addition, there is some niobium pentoxide inside the coating. These niobium compounds originate from the oxidation of the niobium inside the TLM alloy during micro-arc oxidation.

Furthermore, there are some diffraction peaks due to tricalcium phosphate in Fig. 3(a), (b). Tricalcium phosphate (TCP) can dissociate into $PO_4^{3-}$ and $Ca^{2+}$ in body fluid. $PO_4^{3-}$ and $Ca^{2+}$ can promote the formation of new hard tissue and can be absorbed by the human body. Therefore, the TCP phase in the coating can promote biological activity[16]. Compared with rutile, the anatase phase has better lattice matching with apatite crystals in some studies[17]. It has also been reported that the (101) crystal plane of rutile matches well the (200) crystal plane of hydroxyapatite, which can promote nucleation and growth of apatite crystals in some other studies[18-19]. Therefore, depending on the anatase content, the bioactivity of the TLM micro-arc oxidation coating may be better than that of the TC4 coating.

### *3.2 Corrosion resistance*

#### *3.2.1. Potentiodynamic Polarization curves*

We measured the metal corrosion rate by the Tafel extrapolation method[20]. The functional relationship between electrode potential and polarization current density conforms to the famous Tafel

equation. Fig. 4 shows the polarization curves of the treated samples of TC4-MAO and TLM-MAO. The corrosion potential ($E_{corr}$) and the current density ($i_{corr}$) are presented in table 3. The corrosion current density of the TC4-MAO coating, with a value of $8.3546\pm0.0412\times10^{-8}$ A·cm$^{-2}$, is lower than that of TLM, with a value of $4.9191\pm0.0378\times10^{-7}$ A·cm$^{-2}$. However, there is a small difference in the corrosion potential between the two groups. Because the influence of the corrosion current on the corrosion process is more important[21], the corrosion resistance of the TC4-MAO coating is better than that of the TLM micro-arc oxidation film in simulated body fluid. However, an obvious passivation plateau is observed in the TLM-MAO coating, and the TC4-MAO coating has undergone overpassivation, which is not conducive to corrosion resistance. In comparison to the anatase phase, the rutile phase shows better corrosion resistance[22], which is consistent with the XRD analysis.

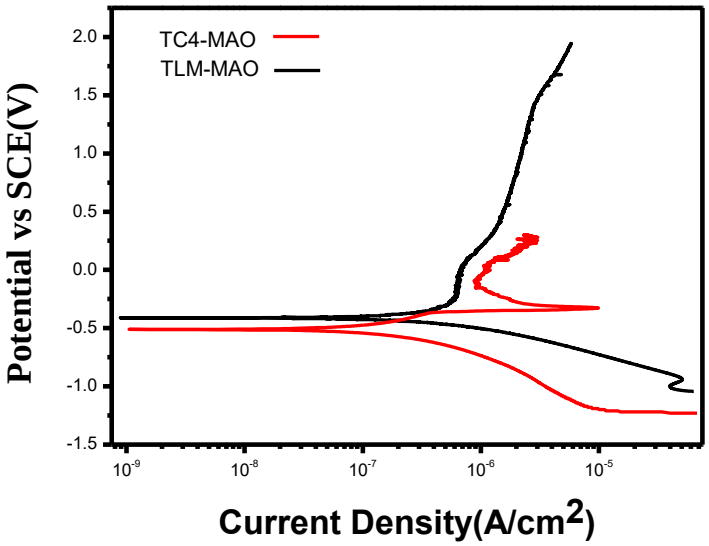


**Figure 4.** Potentiodynamic scan results of the TLM-MAO and TC4-MAO samples in SBF solution at room temperature.

**Table 3.** Values of corrosion potential and current density for all groups in SBF solution

| Group | $E_{corr}$(V) | $i_{corr}$(A cm$^{-2}$) |
|---|---|---|
| **TC4-MAO** | -0.4927±0.0128 | $8.3546\pm0.0412\times10^{-8}$ |
| **TLM-MAO** | -0.4117±0.0312 | $4.9191\pm0.0378\times10^{-7}$ |

*3.2.2 Electrochemical Impedance Spectroscopy*

As seen in the Bode phase diagram (Fig. 5c), the EIS responses of the MAO coatings show two time constants at high frequencies and low frequencies. Fazel[23] considered that this is attributed to the formation of an oxide film consisting of a porous outer layer and a dense inner layer. In the Bode impedance diagram (Fig. 5b), the resistance of the barrier layer of the TLM-MAO coating is lower than that of the TC4 coating, which can be explained by the lower thickness of the barrier layer and the presence of more defects on the TLM alloy than on the TC4 alloy[24]. Moreover, the lower resistance

might be explained by the higher electrical conductivity and solubility of niobium oxide in micro-arc oxidized TLM.

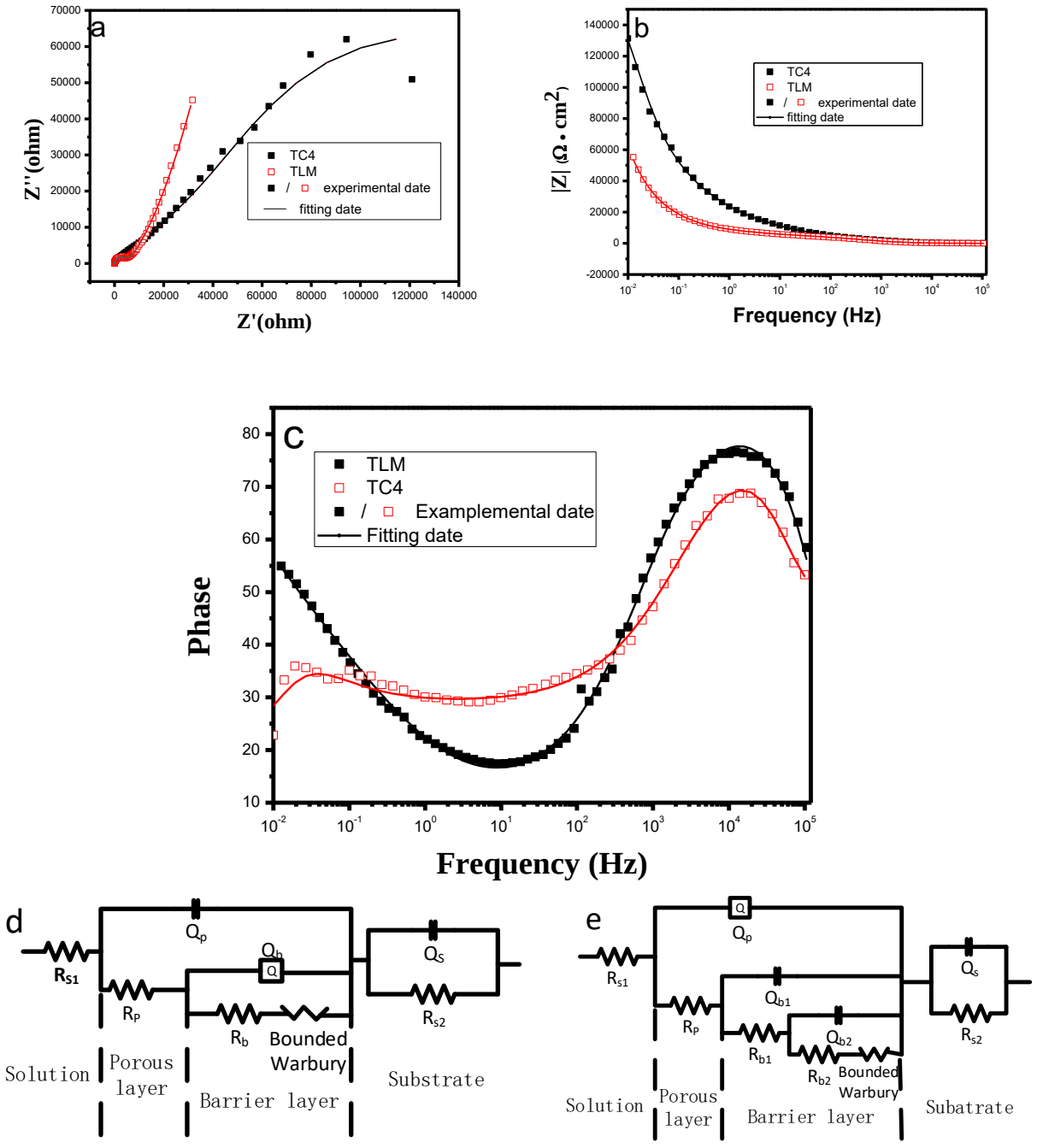


**Figure 5.** EIS evaluations of TC4-MAO and TLM-MAO coating in SBF solution at 37℃: (a) Nyquist plots, (b) Bode impedance plots, (c) Bode phase plots, (d) equivalent circuit model for the TLM-MAO sample and (e) equivalent circuit model for the sample TC4-MAO.

The MAO coating of the TLM alloy is fit to a two-layer oxide model containing an external environment ($R_{s1}$, $R_{s2}$ and $Q_s$), an outer porous oxide layer ($R_p$ and $Q_p$), and an inner dense barrier oxide layer ($R_b$ and $Q_b$). In addition, there is some diffusion evidence in the Nyquist plots, and the

Warburg diffusion element is added to the modified circuit, as shown in Fig. 5e. In some previous studies, the calcium and phosphorus ion transfer processes in oxide coatings can be explained by the Warburg diffusion element[20,21]. In contrast, the equivalent circuit model of the TC4 alloy is different from that of the TLM alloy in the inner dense barrier oxide layer, which adds a parallel circuit behind $R_{b1}$. Some similar equivalent circuits of Ti alloy were proposed by other scholars[21,23].

The fit values for important circuit elements of the TLM-MAO coating and TC4-MAO coating are listed in table 4. The n ($-1 \leq n \leq 1$) index is far from 1, which indicates that the surfaces of both coatings do not have an ideal capacitance[21,25-27]. The $\chi^2$ index shows the chi squared values of each simulated circuit, and the fittings are very good, with $\chi^2$ values close to $10^{-4}$[19]. The resistance of the compact layer ($R_b$) is extraordinarily larger than that of the outer porous layer ($R_s$), so it is a major determinant of the corrosion resistance of MAO coatings. Through qualitative analysis, the $R_b$ of the TC4-MAO coating was determined to be larger than that of the TLM-MAO coating, which indicates that the TC4-MAO coating has better corrosion resistance, which is consistent with the electrodynamic polarization curve results.

**Table 4.** Equivalent circuit element fit values obtained from EIS data for TLM and MAO coatings

| **Group** | $R_{s1}$(Ω ·cm) | $Q_p$-TLM ((μF· $cm^{-2}$) | $n_p$ | $R_p$(KΩ ·$cm^2$) | $CPE_b$-TLM | $R_b$(MΩ ·$cm^2$) | $R_{b1}$(MΩ ·$cm^2$) | $R_{b2}$(MΩ ·$cm^2$) | $\chi^2$ |
|---|---|---|---|---|---|---|---|---|---|
| **TLM** | 14.3 | 0.0651 | 0.374 | 581 | $1.09\times 10^{-5}$ | $7.11\times 10^{3}$ | | | $>8.3\times 10^{-4}$ |
| **Group** | $R_{s1}$ (Ω ·cm) | $CPE_P$-TC4 | $n_p$ | $R_p$(KΩ ·$cm^2$) | $Q_b$-TC4 ((μF· $cm^{-2}$) | $R_b$(MΩ ·$cm^2$) | $R_{b1}$(MΩ ·$cm^2$) | $R_{b2}$(MΩ ·$cm^2$) | $\chi^2$ |
| **TC4** | 15.41 | $2.3\times 10^{-5}$ | 0.322 | 16.43 | 0.0129 | $7.11\times 10^{3}$ | 106.7 | $1.17\times 10^{6}$ | $>1.10\times 10^{-3}$ |

## 4. CONCLUSION

The ceramic coatings were prepared in a $KH_2PO_4$ electrolyte using micro-arc oxidation (MAO), and the ceramic oxide coating was clearly divided into two layers: a dense inner layer and a porous outer layer. Furthermore, XRD indicates that the coating of TLM-MAO consisted mainly of anatase, rutile, $Nb_2O_5$ and CaP, which is helpful for improving the biological activity of the alloy surface, but the rutile content in the TLM coating is lower than that in the TC4 alloy, leading to poorer corrosion resistance. Potentiodynamic polarization curves and electrochemical impedance spectroscopy (EIS) all indicate that the TC4-MAO coating has better corrosion resistance. Moreover, the inner film has better corrosion resistance than the outer layer. In conclusion, the corrosion

resistance of the TC4-MAO coating is better than that of the TLM coating, but the formation rate of hydroxyapatite is lower than that of TLM.

ACKNOWLEDGEMENT
We acknowledge financial support from the undergraduate innovation training programme of Sichuan China(project No:201910615083).

## References

1. Y.M. Wang, D.C. Jia, L.X. Guo, T.Q. Lei and B.L. Jiang, *Mater. Chem. Phys.,* 90 (2005) 128.
2. Y. Luo and G. Chen, *Biological surface modification technology of titanium alloy*, China university of mining and technology press, 2013, Beijing, China.
3. L.H. Li, Y.M. Kong, H.W. Kim, Y.W. Kim, H.E. Kim, S.J. Heo and J.Y. Koak, *Biomaterials*, 25 (2004) 2867.
4. D.D. Deligianni, N. Katsala, S. Ladas, D. Sotiropoulou, J. Amedee and Y.F. Missirlis, *Biomaterials*, 22 (2001) 1241.
5. R. Luo, Z.D. Liu, F.X. Yan, Y. Kong and Y.T. Zhang, *Appl. Surf. Sci.,* 266 (2013) 57.
6. P. Liu, W.Y. Li, J.B. Zhang and Y. Lin, *J. Mater. Res.,* 26 (2011) 1532.
7. E. Matykina, R. Arrabal, B. Mingo, M. Mohedano, A. Pardo and M.C. Merino, *Surf. Coat. Technol.,* 307 (2016) 1255.
8. R.M. Trommer, L.A. Santos and C.P. Bergmann, *Surf. Coat. Technol.,* 201 (2007) 9587.
9. J. Jin, X.H. Li, J.W. Wu and B.Y. Lou, *Rare Met. (Beijing, China),* 37 (2018) 26.
10. J.H. Wang, J. Wang, Y. Lu, M.H. Du and F.Z. Han, *Appl. Surf. Sci.,* 324 (2015) 405.
11. A.F. Yetim, *Surf. Coat.Technol.,* 205 (2010) 1757.
12. S. Stojadinović, R. Vasilić, M. Petković, B. Kasalica, I. Belč, A. Žekić and Lj. Zeković, *Appl. Surf. Sci.,* 265 (2013) 226.
13. Y.X. Tian, Z.T. Yu, J.L. Niu, S. Yu, J.Y. Han, C.C. Liu and B.B. Wen, *Rare Met. Mater. Eng.,* 43 (2014) 132.
14. D.Q. Wei, Y. Zhou, Y.B. Wang, Q.C. Meng and D.C. Jia, *Surf. Coat. Technol.,* 202 (2008) 5012.
15. Z.X. Li, *Preparation Technology and Performance of Ceramic Coatings on Biomedical Ti-6Al-4V Alloys through Micro-arc Oxidation*, Changchun University Of Technology, 2016, Changchun, china.
16. M.D. Roach, R.S. Williamson, I.P. Blakely and L.M. Didier, *Mat. Sci. Eng. C-Mater.,* 58 (2016) 213.
17. J. Domaradzki, D.Kaczmarek, E.L. Prociow, A. Borkowska, D. Schmeisser and G. Beuckert, *Thin Solid Film,* 513 (2006) 269.
18. B. Munirathinam and L. Neelakantan, *Mat. Sci. Eng. C-Mater.,* 49 (2015) 567.
19. B.C. Yang, M. Uchida, H.M. Kim, X.D. Zhang and T. Kokubo, *Biomaterials,* 25 (2004) 1003.
20. H.H. Wang, J.H. Wang and C.W. Fu, *Int. J. Electrochem Sci.,* 8 (2013) 8812.
21. A.C. Alves, F. Wenger, P. Ponthiaux, J.P. Celis, A.M. Pinto, L.A. Rocha and J.C.S. Fernandes, *Electrochim. Acta,* 234 (2017) 16.
22. M. Shokouhfar, C. Dehghanian, M. Montazeri and A. Baradaran, *Appl. Surf. Sci.,* 258 (2012) 2416.
23. M. Fazel, H.R. Salimijazi, M.A. Golozar and M.R. Garsivaz jazi, *Appl. Surf. Sci.,* 324 (2015) 751.
24. E. Matykina, R. Arrabal, M. Mohedano, A. Pardo, M.C. Merino and E. Rivero, *J. Mater. Sci.: Mater. Med.,* 24 (2013) 37.
25. S. Gnedenkov and S. Sinebryukhov, *Russ. J. Electrochem.,* 41 (2005) 858.
26. X.L. Zhang, Z.P. Yao, Z.H. Jiang, Y.F. Zhang and X.W. Liu, *Corros. Sci.,* 53 (2011) 2253.

27. D. Quintero, O. Galvis, J. Calderón, J.G. Castaño and F. Echeverría, *Surf. Coat. Technol.,* 258 (2014) 1223.